THE JOURNAL OF PHYSICAL CHEMISTRY C

Article

pubs.acs.org/JPCC

Nonadiabatic Molecular Dynamics Modeling of the Intrachain Charge Transport in Conjugated Diketopyrrolo-pyrrole Polymers

Xing Gao,[†] Hua Geng,[‡] Qian Peng,[‡] Jiajun Ren,[†] Yuanping Yi,[‡] Dong Wang,[†] and Zhigang Shuai*[,†,‡]

[†]MOE Key Laboratory of Organic OptoElectronics and Molecular Engineering, Department of Chemistry, Tsinghua University, Beijing, 100084, People's Republic of China

[‡]Key Laboratory of Organic Solids, Beijing National Laboratory for Molecular Science (BNLMS), Institute of Chemistry, Chinese Academy of Sciences, Beijing, 100190, People's Republic of China

Supporting Information

ABSTRACT: Understanding the carrier transport processes and predicting the carrier mobility from first principle in organic electronic materials has been a longstanding challenge. We have applied the nonadiabatic Ehrenfest dynamics coupled with density functional tight binding (DFTB) to investigate the carrier motion in the donor−acceptor type polymer for photovoltaics. The equations of motion for the electrons are evolved under the fixed subspace spanned by the active molecular orbitals during each nuclear time step, and the feedback from charge to the nuclei motions, namely, the polaronic effect, is considered. We then use this methodology to investigate the charge transport dynamics for the ladder-type poly(*p*-phenylenes) (LPPP) and poly(diketopyrrolo-pyrrole (DPP)) series with ∼2 × 10^3 atoms. The carrier mobilities are evaluated via the diffusion process. It was found that the diffusion abilities are determined by the magnitude of transfer integrals and localization length for frontier orbital, which is caused by the self-trapping effects (polaron) arising from the double bond stretching and twisting motions. This method can be useful in exploring the underlying charge transport behavior and improving the structure design of materials in organic electronics.

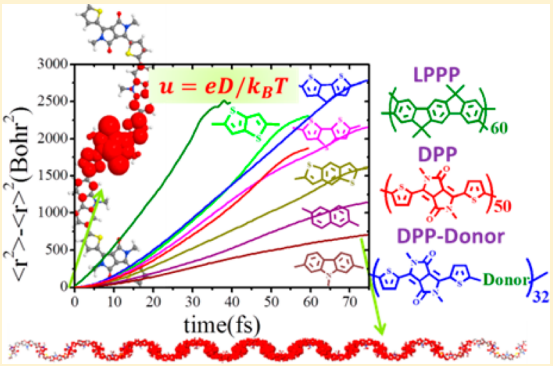

1. INTRODUCTION

Mobility is an important parameter to the performance of organic field effect transistors (OFETs), organic photovoltaics (OPVs)m and organic light emitting diodes (OLEDs).[1−4] Recently, the DPP-based donor−acceptor conjugated copolymers have demonstrated mobility up to 10 cm^2/(V s) for hole and 1 cm^2/(V s) for electron in the OFETs.[5−8] Siebbeles et al. have combined the microwave experiment with one-dimensional diffusion model calculation and shown the mobility in LPPP is estimated to be ∼600 cm^2/(V s).[9,10] The most recent structure probe experiments indicate that the transport behavior in high mobility polymers presents quasi one-dimensional; that is, carrier conduction is mostly along the backbone direction with very few intermolecular hopping through short π-orbital overlap.[11−14] Understanding the intrachain charge transport is the first step to improving the performance or design new material systems in the devices. Therefore, it is of great importance to develop ab initio dynamic methods to simulate the underlying charge transport process and to calculate the charge mobility.

Theoretically, on the basis of model Hamiltonian for organic crystals and conjugated polymers, the mixed quantum/classical (MQC) dynamics[15] have been used to investigate carrier transport mechanism and to evaluate the carrier mobility considering the intramolecular[16] and intermolecular[17] electron−phonon coupling effects. Most recently, Wang and Beljonne have developed the MQC flexible surface hopping dynamics to treat the crossover behavior from hopping to band-like transport regimes in a unified way.[18−20] These methods have all treated the nuclear motions classically. However, the nuclear quantum tunneling effects have been found to be important for charge transport in organic semiconductors and conjugated polymers.[21−23] Nonperturbative hierarchically coupled equations of motion or non-Markovian stochastic Schrödinger equation, which can consider the nuclear quantum effect, have been successfully applied to carrier dynamics in molecular aggregates.[24,25] However, this is either computationally expensive or requires spectral density before the electron dynamics simulation, and also there is no explicit feedback effect from electron to the nuclear. From an ab initio point of view, the multiscale methods combined with static[26] and dynamic disorders[27−29] have been developed to study macroscopic transport behavior in poly(3-hexylthiophene) (P3HT). The intrinsic mobility in a 4802-atom system has been obtained directly by using an integrated tool consisting of large-scale electronic structure calculation, electron dynamics, and classical

Received: December 30, 2013
Revised: February 22, 2014
Published: February 27, 2014

   dx.doi.org/10.1021/jp412782n | J. Phys. Chem. C 2014, 118, 6631−6640

nuclear dynamics.[30] However, the feedback from electrons to the nuclei, that is, the polaronic effect, has been neglected. The recent advances in DFTB approach have been demonstrated as an effective method for treating electronic structure in complex systems.[31−38] Also, it has been successfully combined with MQC nonadiabatic molecular dynamics methods and found multiple applications for charge transfer in DNA,[39−42] nonradiative decay in water molecules,[43] biological basis,[44−46] and as organic molecule with counterintuitive aggregation-induced emission phenomena.[47]

In this work, we focus on the charge transport process in the intrachain conjugated polymer systems, which contain about 10^3 to 2×10^3 atoms. The MQC Ehrenfest dynamics that can take into account the feedback from electrons to the nuclei have been implemented to investigate the detailed charge transport dynamics based on the DFTB electronic structure calculation. From the ensembles of trajectories in the nonadiabatic and Born−Oppenheimer dynamics, the results, such as carrier diffusion behavior, the evolutions of delocalization length for the frontier orbital and internal coordinates, density of states, and the energy autocorrelation functions (ACFs), can be analyzed. The mobilities for the polymers are evaluated directly from the diffusion processes. It is found that the double bond stretching and twisting motions related to the dithienyl-DPP unit mainly caused the orbital localization, modulated the transfer integrals, and affected the mobility in the conjugated polymer.

2. THEORETICAL METHODOLOGY

2.1. Electronic Structure Calculation. The dftb+ code,[48] which was integrated by the Ehrenfest nonadiabatic molecular dynamics, is used to calculate the electronic structure for the polymers on-the-fly. The ith molecular orbital $|\varphi_i\rangle$ can be obtained from the Kohn−Sham (KS) equation $\hat{H}|\varphi_i\rangle = \varepsilon_i|\varphi_i\rangle$, where ε_i is the orbital energy for $|\varphi_i\rangle$. When expressed on atomic basis, the matrices equation $HC = SCE$ is obtained, where H and S represent the Hamiltonian and overlap matrices, respectively. C and E denote wave function and molecular orbital energies. Both H and S are parametrized as a function of adjacent atomic distance for each atomic type. So it is highly efficient for the electronic structure calculation when running the dynamics on-the-fly. On the basis of the KS orbitals from DFTB, the evolution state $|\psi(t)\rangle$ can be constructed as:

$$|\psi(t)\rangle = \sum_{m=1}^{N} a_m(t)|\varphi_m(t)\rangle \tag{1}$$

$a_m(t)$ is the evolution coefficient for the mth state at time t, and N is the total number of KS orbitals.

2.2. Nonadiabatic Dynamics. The evolution state $|\psi(t)\rangle$ follows the time-dependent Kohn−Sham (TDKS) equation:

$$i\hbar\frac{\partial}{\partial t}|\psi(t)\rangle = \hat{H}(t)|\psi(t)\rangle \tag{2}$$

From eqs 1 and 2, we obtain the TDKS equation:

$$i\hbar\frac{\partial}{\partial t}a_n = a_n\varepsilon_n - i\hbar\sum_m a_m\langle\varphi_n(t)|\frac{\partial}{\partial t}|\varphi_m(t)\rangle \tag{3}$$

Generally, the nonadiabatic coupling term $\langle\varphi_n(t)|\partial/(\partial t)|\varphi_m(t)\rangle$ needs to be linearly interpolated between two adjacent time steps ($[t_1, t_2]$) for the nuclear. However, during these time steps, there are many energy level degenerations or crossings within KS orbitals for molecular systems in charge transport, so it is not appropriate to use eq 3 directly. We make the following expansion:

$$|\psi(t)\rangle = \sum_{m=1}^{N} a'_m(t)|\varphi_m(t_1)\rangle \tag{4}$$

where t belongs to $[t_1, t_2]$, and the equation of motion can be written as:

$$\begin{aligned} i\hbar\frac{\partial}{\partial t}a'_n(t) &= \sum_m a'_m(t)\langle\varphi_n(t_1)|\hat{H}(t)|\varphi_m(t_1)\rangle \\ &\equiv \sum_m a'_m(t)H_{nm}(t) \end{aligned} \tag{5}$$

In the following nonadiabatic molecular dynamics, eq 4 is used as the equation of motion for the electron. In this case, the space spanned by the basis $\{|\varphi_1(t_1)\rangle,\cdots|\varphi_m(t_1)\rangle\ldots,|\varphi_N(t_1)\rangle\}$ is fixed between $[t_1, t_2]$, so the numerical problem caused by energy level degeneration or crossing can be avoided. According to the linear-time-dependence approximation for $H(t)$:[30]

$$H(t) = H(t_1) + \frac{t - t_1}{t_2 - t_1}[H(t_2) - H(t_1)] \tag{6}$$

where the matrix elements in Hamiltonian $H(t_1)$ and $H(t_2)$ can be written as:

$$H_{nm}(t_1) = \langle\varphi_n(t_1)|\hat{H}(t_1)|\varphi_m(t_1)\rangle = \delta_{nm} \tag{7}$$

and

$$H_{nm}(t_2) = \langle\varphi_n(t_1)|\hat{H}(t_2)|\varphi_m(t_1)\rangle \tag{8}$$

After the expansion:

$$|\varphi_k(t_2)\rangle = \sum_m b_{mk}|\varphi_m(t_1)\rangle \tag{9}$$

where $b_{mk} = \langle\varphi_m(t_1)|\varphi_k(t_2)\rangle$, the Gram−Schmidt orthogonalization is applied to b_{mk} as the restriction of orthonormal condition $\langle\varphi_k(t_2)|\varphi_l(t_2)\rangle = \delta_{kl}$. Next, $H_{nm}(t_2)$ can be derived as

$$\begin{aligned} H_{nm}(t_2) &= \sum_{kl}\langle\varphi_n(t_1)|\varphi_k(t_2)\rangle\langle\varphi_k(t_2)|\hat{H}(t_2)|\varphi_l(t_2)\rangle \\ &\quad \langle\varphi_l(t_2)|\varphi_m(t_1)\rangle \\ &= \sum_k \varepsilon_k(t_2)b_{nk}b^{\dagger}_{km} \end{aligned} \tag{10}$$

Substituting eq 6 with eqs 7 and 10, $H(t)$ can be calculated through linear interpolation between $H(t_1)$ and $H(t_2)$. From eqs 1, 4, and 9, $|\psi(t_2)\rangle = \sum_m a'_m|\varphi_m(t_1)\rangle = \sum_i a_i|\varphi_i(t_2)\rangle = \sum_i a_i\sum_m b_{mi}|\varphi_m(t_1)\rangle$, we can find the relationship between a'_m and a_i:

$$a'_m = \sum_i b_{mi}a_i \tag{11}$$

To study the charge transport, one electron or hole is added into the system, while the other electrons can be frozen at ground state approximately. In the framework of DFTB, under single electron approximation, the average electronic state energy including dynamic part and ground state part[48] plus nuclear repulsion energy E_{rep} read as

dx.doi.org/10.1021/jp412782n | J. Phys. Chem. C 2014, 118, 6631−6640

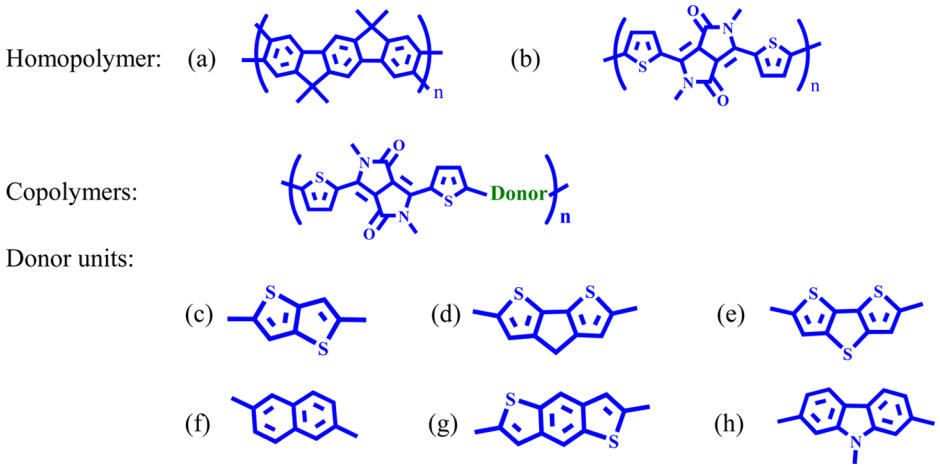

Figure 1. The chemical structures for (a) LPPV, n = 60, (b) DPP_DPP, n = 50, (c) DPP_cTT, (d) DPP_cDT, (e) DPP_f3T, (f) DPP_BDT, (g) DPP_NPT, and (h) DPP_CBZ; for (c)−(g), n = 32.

$$
\begin{aligned}
E^{\text{average}}(t) &= E^{\text{dynamic}} + E^{\text{ground}} \\
&= \langle \psi(t)|\hat{H}|\psi(t)\rangle \\
&\quad + \sum_i f_i \langle \varphi_i(t)|\hat{H}_0|\varphi_i(t)\rangle + \frac{1}{2}\sum_{\alpha,\beta}\gamma_{\alpha\beta}\Delta q_\alpha \Delta q_\beta \\
&\quad + E_{\text{rep}}
\end{aligned} \tag{12}
$$

where f_i is the occupation number for the ith orbital frozen at ground state, and $\gamma_{\alpha\beta}$ is a parameter depending on the Hubbard parameters of atoms α and β and the distance between the two atoms. Δq_α, Δq_β represent Mulliken charge fluctuations on isolated atoms α, β, respectively, and can be evaluated self-consistently. Nuclei are treated classically and can be derived according to Newton equation of motion. The force $\mathbf{F}_\alpha$ as the derivative of E^{average} in the Ehrenfest dynamics applied to the nuclear α can be written as

$$
\begin{aligned}
\mathbf{F}_\alpha &= -\nabla_{\mathbf{R}_\alpha} E^{\text{average}}(t) = \mathbf{F}_\alpha^{\text{dynamic}} + \mathbf{F}_\alpha^{\text{ground}} \\
&= -\sum_{\mu\nu} \rho'_{\nu\mu}(t)\nabla_{\mathbf{R}_\alpha} H^0_{\mu\nu} - \left(\rho'^{\varepsilon}_{\nu\mu}(t) - \frac{H^1_{\mu\nu}}{S_{\mu\nu}}\right)\nabla_{\mathbf{R}_\alpha} S_{\mu\nu} \\
&\quad - \sum_{\mu\nu} \rho'_{\nu\mu}(t)\frac{1}{2}S_{\mu\nu}\nabla_{\mathbf{R}_\alpha}(\gamma_{\delta\alpha} + \gamma_{\beta\alpha})\Delta q_\alpha \\
&\quad - \sum_{\mu\nu} \rho_{\nu\mu}(t)\nabla_{\mathbf{R}_\alpha} H^0_{\mu\nu} - \left[\rho^{\varepsilon}_{\nu\mu}(t) - \frac{H^1_{\mu\nu}}{S_{\mu\nu}}\rho_{\nu\mu}(t)\right]\nabla_{\mathbf{R}_\alpha} S_{\mu\nu} \\
&\quad - \Delta q_\alpha(t)\sum_\zeta^N \nabla_{\mathbf{R}_\alpha}\gamma_{\alpha\zeta}\Delta q_\zeta(t) - \nabla_{\mathbf{R}_\alpha} E_{\text{rep}}
\end{aligned} \tag{13}
$$

which is similar to the ground-state force calculation,[48] and the dynamic part $\mathbf{F}_\alpha^{\text{dynamic}}$ from $\langle \psi(t)|\hat{H}|\psi(t)\rangle$ can be derived and shown in the Supporting Information, where $\rho_{\nu\mu}' \equiv \sum_m c_{\nu m} a_m^\dagger(t) a_m(t) c_{m\mu}^\dagger$, $\rho_{\nu\mu}(t) \equiv \sum_m f_m c_{\nu m} c_{m\mu}^\dagger$ and $\rho'^{\epsilon}_{\nu\mu} = \sum_m c_{\nu m} a_m^\dagger(t)\epsilon_m c_{m\mu}^\dagger$, $\rho^{\epsilon}_{\nu\mu}(t) \equiv \sum_m f_m \epsilon_m c_{\nu m} c_{m\mu}^\dagger$ correspond to the density matrix and energy weighted density matrix, respectively. $a_m(t)$ can be determined according to the electron equation of motion eqs 5 and 11. $H^0_{\mu\nu} \equiv \langle \phi_\mu|\hat{H}_0|\phi_\nu\rangle$ and $H^1_{\mu\nu} \equiv 1/2S_{\mu\nu}\sum_\zeta^N(\gamma_{\alpha\zeta} + \gamma_{\beta\zeta})\Delta q_\zeta$ denote zero-order Hamiltonian and self-consistent charge terms, respectively.[48] The density matrices are updated at each nuclear time step, and the derivatives of $H^0_{\mu\nu}$, $S_{\mu\nu}$, E_{rep}, and $\gamma_{\alpha\zeta}$ are evaluated numerically in the original dftb+ code; the parameter set mio-1-1 is used in this work.

3. RESULTS AND DISCUSSION

3.1. Initial State for Electron Dynamics. To elucidate the structure−property relationship, we investigate eight kinds of single chain polymers with chemical structures shown in Figure 1. There are two kinds of homopolymers, LPPP and poly dithienyl-DPP (DPP_DPP), consisting of 60 and 50 monomers, respectively. The rest are copolymers each with 32 monomers, which consist of the same acceptor dithienyl-DPP unit and different kinds of donor units as thienothiophene (DPP_cTT), cyclopentadithiophene (DPP_cDT), dithienothiophene (DPP_f3T), benzodithiophene (DPP_BDT), naphthalene (DPP_NPT), and carbazole (DPP_CBZ). The oligomer length is chosen according to the fact that the charged carrier is expected not to reach the boundary within the simulation time. There are about 10^3 to 2×10^3 atoms in total for each polymer chain. We optimize the dimer structure using the Gaussian 09 package[49] with B3LYP functional and 6-31G(d, p) basis sets and extend to one-dimensional chain with the desired number of units. It should be noted that the side chain is neglected because we did not consider the intermolecular packings.[7,50−54]

We expand the hole wavepacket in the subspace of occupied orbitals. We choose 120 and 50 eigenstates for LPPP and DPP_DPP, respectively, and 32 eigenstates for other copolymers. The charge conservation is carefully checked to ensure this subspace spanned by the eigenstates is complete for the expansion. The initial hole state is prepared with location at the central unit of the polymer through projecting the HOMO orbital in the monomer into the subspace. The charge mainly centers on the dithienyl-DPP unit, while it uniformly distributes along the central unit of the backbone for LPPP. The detailed charge distribution for the initial hole state of each polymer is shown in Figure S1 in the Supporting Information.

3.2. Nonadiabatic Dynamics for the Electrons and Nuclei. Considering the nonadiabatic dynamics, the initial velocities for the nuclei are randomly sampled according to Boltzmann distribution with temperature at 500 K. Because of the structure relaxation, the temperature will decrease to

dx.doi.org/10.1021/jp412782n | J. Phys. Chem. C 2014, 118, 6631−6640

around 300 K at the diffusion region for the charge transport. After the initial conditions are assigned, the electron equations of motion are solved by the eighth order Runge−Kutta method with adjustable time step by using the rksuite_90 package,[55] while simultaneously the equations of motion for the nuclei are solved using the velocity Verlet algorithm with a time step of 0.5 fs. In this case, the polaron effect is naturally considered during the nonadiabatic dynamics. It is interesting to compare our result with that from literature, which has shown a negligible polaron effect on the charge transport in high mobility molecular systems based on the simulation with the Su−Schrieffer−Heeger (SSH) model.[56] Because of the differences in diffusion velocities for the polymers, the total time scale for each polymer is tested. Also, the time scales for LPPP, DPP_DPP, and DPP_cTT are 40, 50, and 60 fs, respectively, while for the other polymers it is 75 fs. The nonadiabatic molecular dynamics then are started from the initial conditions prepared above with 100 trajectories for each polymer. The number for the trajectory has been tested to ensure the convergence. The diffusion distance test for DPP_CBZ copolymer with 50, 100, and 200 trajectories can be referred to as Figure 2S in the Supporting Information. In the following section, besides the ensemble averaging over 100 trajectories, we have also sampled enough number of points along each trajectory to the average.

The charge mobility can be evaluated from the nonadiabatic dynamics directly. First, the hole displacement $\mathbf{r}(t)$ and square of the displacement $\mathbf{r}^2(t)$ are approximately calculated by $\mathbf{r}(t) = \langle\psi(t)|\mathbf{r}|\psi(t)\rangle \approx \sum_\mu |a_\mu(t)|^2\mathbf{R}_\alpha$ and $\mathbf{r}^2(t) = \langle\psi(t)|\mathbf{r}|\psi(t)\rangle \approx \sum_\mu |a_\mu(t)|^2\mathbf{R}_\alpha^2$, respectively. Second, the mean displacement (MD) and square of the displacement (MSD) are obtained through ensemble average over 100 trajectories. The variance of the displacement for the hole in each polymer is shown in Figure 2.

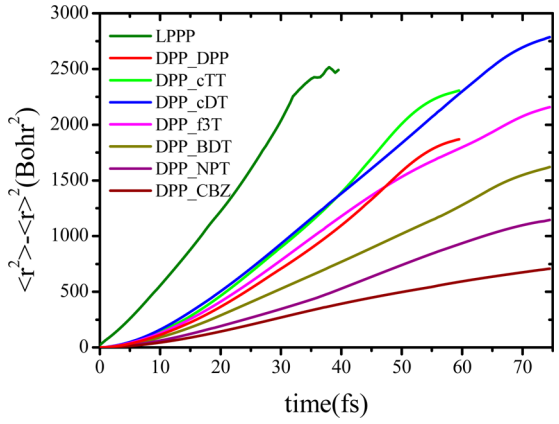

Figure 2. Variance of diffusion distance averaged from ensembles of 100 trajectories of the nonadiabatic dynamics for the LPPP, homo-DPP polymer (DPP_DPP), and DPP copolymers, respectively.

There are three stages that can be found in the diffusion curve. It takes about 15 fs to experience the initial transition stage for each polymer. The curves in this stage are parabolic-like and similar to the inertial regimes for classical particles.[57] After that, the curves are linear versus time, suggesting that the diffusion regime takes over this stage. In about 5 fs, the hole will reach the chain end and go into the plateau regime. When the system evolves into the diffusion regime, the diffusion constant $D = 1/2nt(\langle\mathbf{r}^2(t)\rangle - \langle\mathbf{r}(t)\rangle^2)$ (n is the dimension for the space) is evaluated by substituting the equation with MD and MSD for each polymer. Finally, according to the Einstein diffusion equation, the carrier mobility $\mu = eD/k_BT$, where e is the charge for the carrier, k_B is Boltzmann constant, and T is temperature. The intrachain hole mobilities obtained for each polymer are listed in Table 1. The mobility for LPPP is 50 $cm^2/(V\ s)$, which is about 1 order of magnitude smaller than that by Siebbeles et al.[9] In the latter work, first, the time-resolved microwave conductivity experiment was applied to measure the AC mobility for finite polymer chains. They observed chain length dependence for the high-frequency mobility. To consider the chain ends effect, the polymer chain then was modeled by a flat energy surface between infinitely high reflecting barriers, and the one-dimensional diffusion equation was used to obtain the charge carrier diffusion distance. In the end, the intrachain mobility for infinite chain length was extrapolated to be 600 $cm^2/(V\ s)$ based on the experimental results. However, in practical experiment, there is always a conjugation break existing in the polymer chains as shown by Scholes et al.[58] Besides, during the diffusion process, the energy surface for the charge carrier in the conjugated polymer is usually curved, not flat. For the DPP-based homopolymer, DPP_DPP, the hole mobility is calculated to be 27 $cm^2/(V\ s)$. In the case of donor−acceptor copolymer, the mobility depends on the kind of donor unit in the polymer chain. The highest and the lowest mobilities are 34 (DPP_cTT) and 5 (DPP_CBZ) $cm^2/(V\ s)$, respectively. It is found that hole mobility for donor−acceptor copolymers (except for DPP_cTT) is usually less than homopolymer. This is in agreement with the microwave conductivity experiment for polydiacetylene-based copolymers.[59]

The delocalization length at the mobility edge is important to charge transport. The evolution of the highest occupied molecular orbital (HOMO) delocalization length (L) is shown in Figure 3a. The L is averaged from an ensemble of 100 trajectories for each polymer and calculated as $L = 1/\sum_{\alpha=1}|c_\alpha|^4$, where c_α is the wave function based on the αth orthonormal atomic basis set. For all of the polymers considered here, the wave functions first localize in the initial ∼5 fs, and then oscillate with decreased amplitude in the following evolution. The period for the oscillation is estimated to be 21 fs (∼1587 cm^{-1}) as indicated in the figure. This value suggests the importance of double bond stretching motion in coupling to the charge motion and causing the localization. The curves in the figure located from top to down correspond to the increasing wave function localization. Generally, this order is consistent with that for the magnitude of hole mobilities listed in Table 1; that is, the more delocalized is the orbital, the larger is the mobility for the polymer. To further illustrate the HOMO delocalization, the charge distributions along the

Table 1. Absolute Mobility for the Polymers Calculated from the Linear Region in Figure 2

	molecule							
	LPPP	DPP_DPP	DPP_cTT	DPP_cDT	DPP_f3T	DPP_BDT	DPP_NPT	DPP_CBZ
mobility ($cm^2/(V\ s)$)	50	27	34	25	20	14	11	5

dx.doi.org/10.1021/jp412782n | J. Phys. Chem. C 2014, 118, 6631−6640

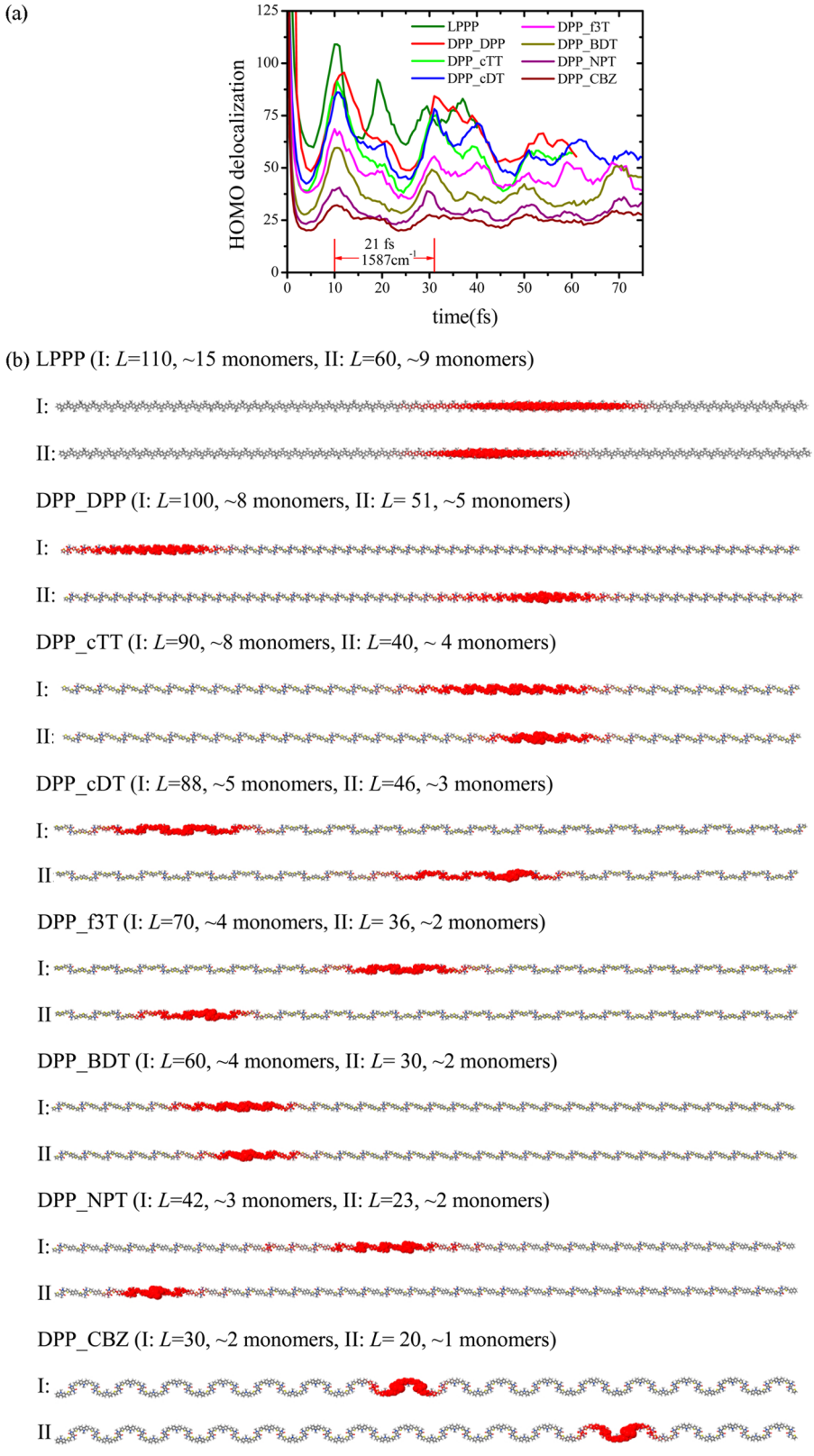

Figure 3. (a) HOMO delocalization (L) averaged over ensembles of 100 trajectories for the conjugated polymers, the oscillation period (~21 fs) corresponds to the stretching motion; and (b) charge distribution along the polymer chains with relevant L and estimated number of monomers. The values in the parentheses for L with I and II for each polymer are sampled at 10 and 25 fs in (a) corresponding to the most delocalized and localized band edge state.

polymer chains are plotted in Figure 3b. The numbers of monomers occupied by the orbitals are estimated and with their corresponding value of L are also shown in the parentheses for each polymer in Figure 3b. The red color indicates the charge distribution. So it can be seen from Figure 3a and b that the effective conjugation lengths are within 15−9 monomers for

dx.doi.org/10.1021/jp412782n | J. Phys. Chem. C 2014, 118, 6631−6640

LPPP, 8−5 for DPP_DPP, while in copolymers they are within 8−4 for DPP_cTT, 5−3 for DPP_NDT, 4−2 for DPP_f3T, 4−2 for DPP_BDT, 3−2 for DPP_NPT, and 2−1 for DPP_CBZ during the diffusion regime.

The densities of states (DOS) for the energies from the top 32 valence orbitals sampled from all of the trajectories are plotted in Figure 4a for LPPP and in Figure 4b for polymers

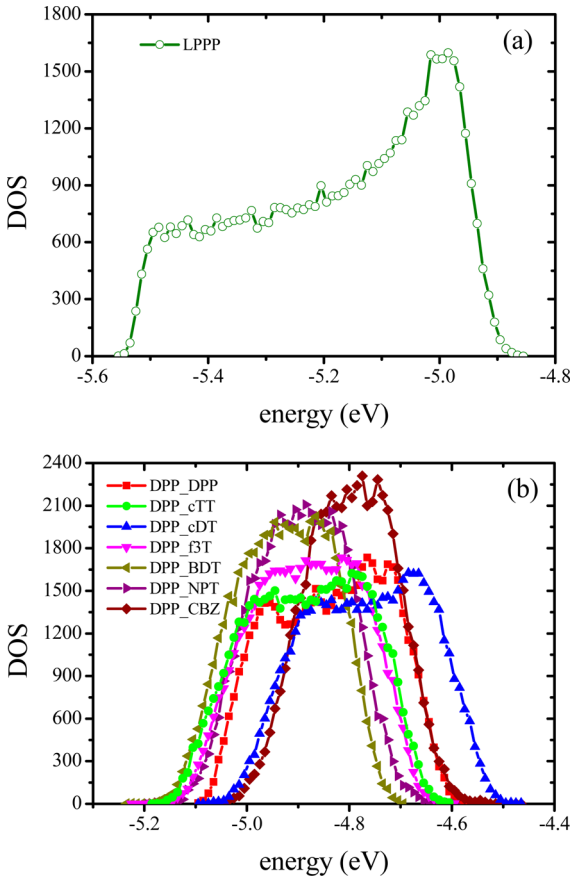

Figure 4. Densities of states from the top 32 valence orbital energies for different polymers.

with DPP unit. The energies are sampled from the diffusion regime during the nonadiabatic dynamics, and the DOS are obtained by directly counting the number of states falling between the given energy intervals. Two tails can be found at each side of the DOS profile for each polymer. These tail states can be attributed to fluctuations of orbital energies at the band edge. The higher mobility system favors a shallower band edge. Here, the contribution from the fluctuations of HOMO orbital energies to the total DOS is shown in Figure 3S in the Supporting Information. The DOS for HOMO follow Gaussian distribution. The full width at half-maximum (fwhm) estimated for HOMO is about 60−100 meV for each polymer. The fwhms for the total orbitals considered are listed in Table 2. There are two factors contributing to the broadening of energy levels. One is the renormalization by the electron−phonon couplings; the other comes from the orbital interactions, transfer integral. To gauge the relative contributions, that the bandwidths evolve with time is plotted in Supporting Information Figure 4S. The bandwidths oscillate with a period of ∼20 fs, which is in agreement with the double bond stretching mode. The largest amplitude for the oscillation is estimated to be ∼55 meV. So it means the magnitude from electron−phonon coupling in different polymers is comparable and estimated to be several dozens of millielectronvolt. So the bandwidths listed in Table 2 corresponding to the broadening of total energy levels largely governed the transfer integral between adjacent monomer in the polymer. The larger bandwidth presents larger transfer integral and then shows higher charge mobility in the polymer. The mobilities versus bandwidths are plotted in Supporting Information Figure 5S. The relationship appears to be roughly linear, which is consistent with the diffusion behavior for charge carrier in a strong electronic coupling regime.

Now we discuss the evolution of typical dihedral angles and bond lengths, which have been taken as an ensembles average from 100 trajectories. The positions for the typical internal coordinates are labeled with red in the chemical structures and are shown in the insets in Figure 5a−f. The standard deviation (SD) of dihedral angles σ_1 and σ_2 versus time is plotted in Figure 5a and b, respectively. The dihedral angle σ_1 in LPPP denotes the twisting motion between two adjacent benzene rings. In the first 15 fs, the SD of σ_1 in LPPP increases fast to 6°, and then it keeps at this degree with small oscillations. When considering P-DPPs, the SDs of σ_1, which denote the twisting motion of thiophene rings in the DPP unit, increase fast to ∼8° in less than 15 fs and then increase slowly with fluctuations between ∼5° and ∼10°. Similarly, in Figure 5b, there are also two stages that can be found for rotations of σ_2. In LPPP, the dihedral angles represent the out-of-plane torsion for benzene rings with amplitude from ∼ −4° to ∼4°. In P-DPPs, the dihedral angles represent the rotations between DPP units and donor units. In the first 15 fs, these angles rotate with fast increasing amplitudes up to 6°; in the following periods, the amplitudes change slowly up to the range of ∼10° at the end of the simulation time. Although the fluctuation amplitudes of σ_1 and σ_2 are within ∼10°, the transfer integrals could take significant decrement because of the randomness for the distribution of the angles.[60,61] Also, it is anticipated that these torsions can further take an important part in localizing the charge distribution and coupling to the carrier motion corresponding to the diffusion regime as shown in Figures 2 and 3.

The stretching motions for different bonds are appended in Figure 5c−e. For LPPP, as shown in Figure 5c and d, the bond lengths are ∼1.47 and ∼1.40 Å with oscillation frequencies of ∼24 fs (1388 cm^{-1}) and ∼19 fs (1754 cm^{-1}), respectively. The oscillation amplitudes change ∼0.01 Å during the diffusion regime. For the P-DPPs, the C═C stretching motions in Figure 5c and d show obvious increments in oscillation amplitudes with frequencies of ∼23 fs (1449 cm^{-1}). Similar behavior could also be found for C−N stretching motion with

Table 2. Bandwidth for the Polymers Estimated from the Full-Width at Half-Maximum (fwhm) in Figure 4

	molecule							
	LPPP	DPP_DPP	DPP_cTT	DPP_cDT	DPP_f3T	DPP_BDT	DPP_NPT	DPP_CBZ
fwhm (meV)	600	370	365	377	362	279	268	242

dx.doi.org/10.1021/jp412782n | J. Phys. Chem. C 2014, 118, 6631−6640

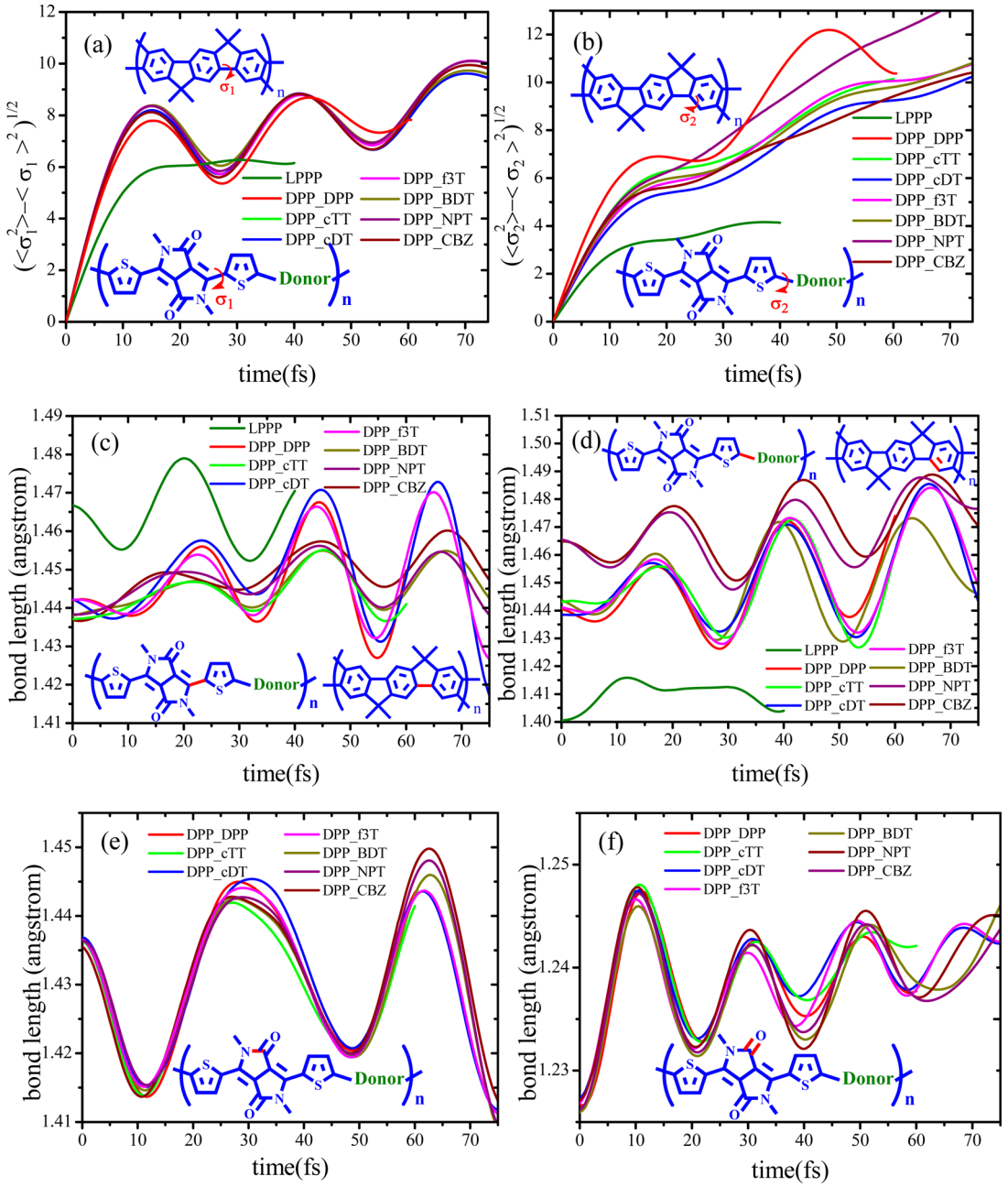

Figure 5. Temporal evolution of standard deviation for the typical dihedral angles for (a) σ_1, (b) σ_2, and average bond lengths for (c) C═C, (d) C═C, (e) C−N, and (f) C═O indicated with red color in the chemical structures for different polymers in the insets.

frequency of ∼32 fs (1042 cm^{-1}) in Figure 5e. Interestingly, the inverse process with decreasing amplitude can be found for C═O stretching motion of ∼20 fs (1666 cm^{-1}). The increasing and decreasing amplitudes indicate the excitation and relaxation processes for the vibrational modes. Also, the locations for these bonds are in general consistent with the charge distributions as shown in Figure 3b and Supporting Information Figure 1S. Combing these two aspects, we can infer that the feedback from electrons to the phonons is important and the polaronic effect cannot be neglected during the carrier diffusion in the P-DPPs.

3.3. Born−Oppenheimer Dynamics. To identify the overall phonon modes contributing to the electron−phonon couplings, the ACFs for the HOMO energy levels and the correspond Fourier transformed (FT) results are reported in Figure 6. The ACFs are obtained by starting the Born−Oppenheimer dynamics with a time scale of 400 fs and a step of 0.1 fs for the nuclear motion. The initial settings for the geometries, velocities, and temperature are the same as the nonadiabatic dynamics. The ACFs can be calculated as:

$$\mathrm{ACF} = \frac{\langle C_{EE}(n\Delta t)\rangle}{\langle C_{EE}(0)\rangle} \tag{14}$$

where

$$C_{EE}(n\Delta t) = \frac{1}{M-n}\sum_{m=1}^{M-n} E(m\Delta t)E((m+n)\Delta t) \tag{15}$$

E is the HOMO energy, M is the number for the total sampling points along the trajectory, and Δt is the nuclear time step. The

dx.doi.org/10.1021/jp412782n | J. Phys. Chem. C 2014, 118, 6631−6640

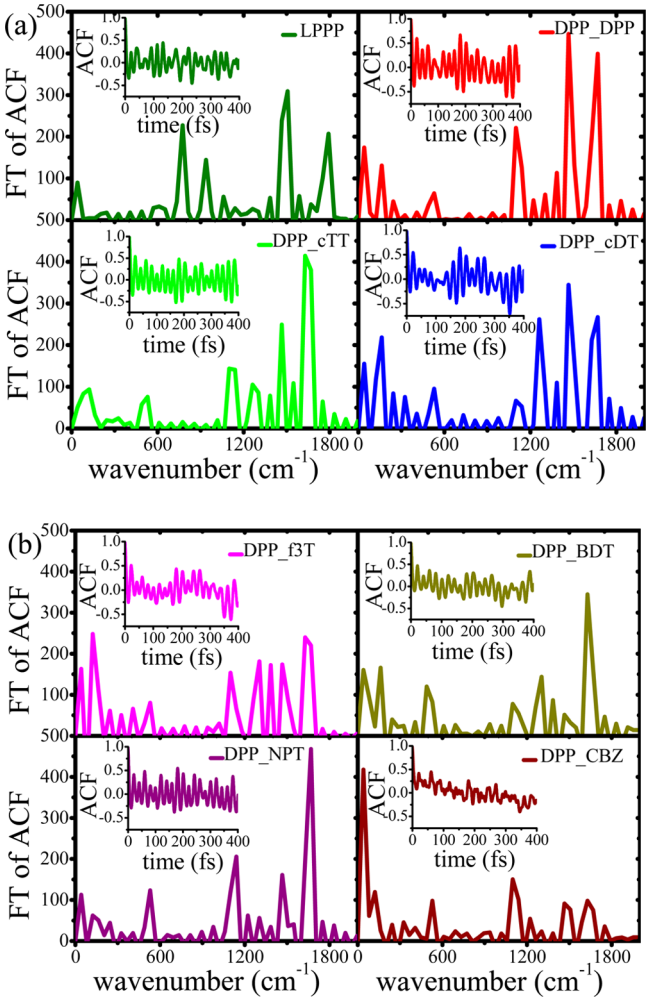

Figure 6. The Fourier transforms (FT) of the energy autocorrelation functions (ACFs) from Born−Oppenheimer dynamics. The corresponding ACFs are shown in the insets.

ACFs show fast decay (<10 fs) and oscillations around zero value, which indicate the possible thermal fluctuations caused memory loss and the establishments of equilibrium states. For P-DPPs, the peaks ranging from ∼1400 to ∼1800 cm^{-1} can be attributed to C═C and C═O stretching motions, while the modes from ∼1100 to ∼1300 cm^{-1} probably come from the single bonds stretching motions like C−N, C−C. One example for the C−N stretching is shown in Figure 5e. The low frequencies with wavenumber less than 300 cm^{-1} give longer than 100 fs rotation periods. The peaks located at this region show small values except for DPP_CBZ. Similar results can be found in LPPP, which show much smaller low frequency contributions because of the locking by the single bonds for the torsions. From the frequency domain results, we can find that the stretching motions with high frequencies take a major part in electron−phonon coupling, while the torsions with low frequencies take a minor part except for DPP_CBZ.

4. CONCLUSIONS

To summarize, we have carried out a nonadiabatic dynamics simulation considering polaronic effects for the hole transport in polymer chains of LPPP and P-DPPs with 10^3 to 2×10^3 atoms. The charge mobilities are calculated according to the Einstein diffusion equation through fitting the linear region of diffusion curves. We find that the intrachain mobility in LPPP is ∼50 $cm^2/(V\ s)$, while in P-DPPs it ranges from ∼30 to ∼5 $cm^2/(V\ s)$ depending on the different donor units. There are two major effects that contribute to the differences in transport abilities. One is the strength of transfer integral between the adjacent monomers, which is modulated by the random fluctuations of typical dihedral angles. The other is the localization length for frontier orbital, which is determined by the strength of electron−phonon couplings induced by the stretching and twisting motions related to DPP units. Our work demonstrated that this methodology is useful in understanding the charge transport process and predicting the mobility from first principle. However, there are two points that should be noted when predicting the carrier mobility. One is our investigation here is confined to a single polymer chain. The interaction of the charge carriers with their polar dielectric environment is neglected now, which can be very important to charge transport as shown by experimental and other theoretical works, in which the interactions have been described in the form of Fröhlich polaron.[62−65] The other is that the simulation now is focusing on intrachain transport, "through bond" diffusion. The "through space" component arising from coupled polymer segments is often the velocity deterministic step during the charge transport, so it is also very important to the mobility prediction. The interchain charge transport in "kinked" chains is being actively pursued.

■ ASSOCIATED CONTENT

Supporting Information

Additional details about derivation of force calculation from dynamic part, the charge distribution of initial hole wavepacket, the convergence test for diffusion distance in DPP_CBZ copolymer, the contribution of HOMO in the total orbital DOS distribution, time evolution for the bandwidth, and the relationship between charge mobility and bandwidth in different copolymers. This material is available free of charge via the Internet at http://pubs.acs.org.

■ AUTHOR INFORMATION

Corresponding Author

*E-mail: zgshuai@tsinghua.edu.cn.

Notes

The authors declare no competing financial interest.

■ ACKNOWLEDGMENTS

We thank Professor Lin-Wang Wang for helpful discussions. This work was supported by the National Natural Science Foundation of China (Grant nos. 21290191 and 91333202), the Ministry of Science and Technology of China through 973 program (Grant nos. 2011CB932304, 2013CB933503), and Tsinghua University Research Foundation (Grant no. 20121088041). The computation in this work was performed on the "Explorer 100" cluster system of Tsinghua National Laboratory for Information Science and Technology.

■ REFERENCES

(1) Coropceanu, V.; Cornil, J.; Da Silva, D. A.; Olivier, Y.; Silbey, R.; Bredas, J. L. Charge Transport in Organic Semiconductors. *Chem. Rev.* **2007**, *107*, 926−952.

(2) Forrest, S. R. The Path to Ubiquitous and Low-Cost Organic Electronic Appliances On Plastic. *Nature* **2004**, *428*, 911−918.

(3) Hains, A. W.; Liang, Z. Q.; Woodhouse, M. A.; Gregg, B. A. Molecular Semiconductors in Organic Photovoltaic Cells. *Chem. Rev.* **2010**, *110*, 6689−6735.
(4) Shuai, Z.; Wang, L.; Li, Q. Evaluation of Charge Mobility in Organic Materials: From Localized to Delocalized Descriptions at a First-Principles Level. *Adv. Mater.* **2011**, *23*, 1145−1153.
(5) Li, J.; Zhao, Y.; Tan, H. S.; Guo, Y.; Di, C.; Yu, G.; Liu, Y.; Lin, M.; Lim, S. H.; Zhou, Y.; et al. A Stable Solution-Processed Polymer Semiconductor with Record High-Mobility for Printed Transistors. *Sci. Rep.* **2012**, *2*, 754.
(6) Nielsen, C. B.; Turbiez, M.; McCulloch, I. Recent Advances in the Development of Semiconducting DPP-Containing Polymers for Transistor Applications. *Adv. Mater.* **2013**, *25*, 1859−1880.
(7) Kang, I.; Yun, H.; Chung, D. S.; Kwon, S.; Kim, Y. Record High Hole Mobility in Polymer Semiconductors via Side-Chain Engineering. *J. Am. Chem. Soc.* **2013**, *135*, 14896−14899.
(8) Chen, Z.; Mi, J. L.; Shahid Ashraf, R.; Yun, G.; Albert-Seifried, S.; Meedom Nielsen, M.; Schroeder, B.; Anthopoulos, T. D.; Heeney, M.; McCulloch, I.; et al. High-performance Ambipolar Diketopyrrolopyrrole-Thieno[3,2-b]thiophene Copolymer Field-effect Transistors with Balanced Hole and Electron Mobilities. *Adv. Mater.* **2012**, *24*, 647−652.
(9) Prins, P.; Grozema, F. C.; Schins, J. M.; Patil, S.; Scherf, U.; Siebbeles, L. High Intrachain Hole Mobility On Molecular Wires of Ladder-Type Poly(p-Phenylenes). *Phys. Rev. Lett.* **2006**, *96*, 146601.
(10) Grozema, F. C.; Siebbeles, L. D. A. Charge Mobilities in Conjugated Polymers Measured by Pulse Radiolysis Time-Resolved Microwave Conductivity: From Single Chains to Solids. *J. Phys. Chem. Lett.* **2011**, *2*, 2951−2958.
(11) Takacs, C. J.; Treat, N. D.; Kraemer, S.; Chen, Z.; Facchetti, A.; Chabinyc, M. L.; Heeger, A. J. Remarkable Order of a High-Performance Polymer. *Nano Lett.* **2013**, *13*, 2522−2527.
(12) Noriega, R.; Rivnay, J.; Vandewal, K.; Koch, F. P. V.; Stingelin, N.; Smith, P.; Toney, M. F.; Salleo, A. A General Relationship Between Disorder, Aggregation and Charge Transport in Conjugated Polymers. *Nat. Mater.* **2013**, *12*, 1038−1044.
(13) Street, R. A. Unraveling Charge Transport in Conjugated Polymers. *Science* **2013**, *341*, 1072−1073.
(14) Xinran, Z.; Bronstein, H.; Kronemeijer, A. J.; Smith, J.; Kim, Y.; Kline, R. J.; Richter, L. J.; Anthopoulos, T. D.; Sirringhaus, H.; Song, K.; et al. Molecular Origin of High Field-Effect Mobility in an Indacenodithiophene-Benzothiadiazole Copolymer. *Nat. Commun.* **2013**, *4*, 2238.
(15) Tully, J. C. Mixed Quantum-Classical Dynamics. *Faraday Discuss.* **1998**, *110*, 407−419.
(16) Stafstrom, S. Electron Localization and the Transition From Adiabatic to Nonadiabatic Charge Transport in Organic Conductors. *Chem. Soc. Rev.* **2010**, *39*, 2484−2499.
(17) Troisi, A. Charge Transport in High Mobility Molecular Semiconductors: Classical Models and New Theories. *Chem. Soc. Rev.* **2011**, *40*, 2347−2358.
(18) Wang, L.; Beljonne, D. Flexible Surface Hopping Approach to Model the Crossover From Hopping to Band-Like Transport in Organic Crystals. *J. Phys. Chem. Lett.* **2013**, *4*, 1888−1894.
(19) Wang, L.; Beljonne, D. Charge Transport in Organic Semiconductors: Assessment of the Mean Field Theory in the Hopping Regime. *J. Chem. Phys.* **2013**, *139*, 064316.
(20) Wang, L.; Guangjun, N.; Xiaodi, Y.; Qian, P.; Qikai, L.; Shuai, Z. Computational Methods for Design of Organic Materials with High Charge Mobility. *Chem. Soc. Rev.* **2010**, *39*, 423−434.
(21) Nan, G.; Yang, X.; Wang, L.; Shuai, Z.; Zhao, Y. Nuclear Tunneling Effects of Charge Transport in Rubrene, Tetracene, and Pentacene. *Phys. Rev. B* **2009**, *79*, 115203.
(22) Geng, H.; Peng, Q.; Wang, L.; Li, H.; Liao, Y.; Ma, Z.; Shuai, Z. Toward Quantitative Prediction of Charge Mobility in Organic Semiconductors: Tunneling Enabled Hopping Model. *Adv. Mater.* **2012**, *24*, 3568−3572.
(23) Asadi, K.; Kronemeijer, A. J.; Cramer, T.; Koster, L. J. A.; Blom, P. W. M.; de Leeuw, D. M. Polaron Hopping Mediated by Nuclear Tunnelling in Semiconducting Polymers at High Carrier Density. *Nat. Commun.* **2013**, *4*, 1710.
(24) Wang, D.; Chen, L.; Zheng, R.; Wang, L.; Shi, Q. Communications: A Nonperturbative Quantum Master Equation Approach to Charge Carrier Transport in Organic Molecular Crystals. *J. Chem. Phys.* **2010**, *132*, 081101.
(25) Zhong, X.; Zhao, Y. Non-Markovian Stochastic Schrödinger Equation at Finite Temperatures for Charge Carrier Dynamics in Organic Crystals. *J. Chem. Phys.* **2013**, *138*, 014111.
(26) Vukmirovic, N.; Wang, L. Charge Carrier Motion in Disordered Conjugated Polymers: A Multiscale Ab Initio Study. *Nano Lett.* **2009**, *9*, 3996−4000.
(27) Zhang, X.; Li, Z.; Lu, G. First-Principles Determination of Charge Carrier Mobility in Disordered Semiconducting Polymers. *Phys. Rev. B* **2010**, *82*, 205210.
(28) Li, Z.; Zhang, X.; Zhang, Y.; Woellner, C. F.; Kuik, M.; Liu, J.; Nguyen, T.; Lu, G. Hole Transport in Diketopyrrolopyrrole (DPP) Small Molecules: A Joint Theoretical and Experimental Study. *J. Phys. Chem. C* **2013**, *117*, 6730−6740.
(29) Li, H.; Duan, L.; Sun, Y.; Zhang, D.; Wang, L.; Qiu, Y. Study of the Hole and Electron Transport in Amorphous 9,10-Di-(2′-naphthyl)anthracene: The First-Principles Approach. *J. Phys. Chem. C* **2013**, *117*, 16336−16342.
(30) Ren, J.; Vukmirovic, N.; Wang, L. Nonadiabatic Molecular Dynamics Simulation for Carrier Transport in a Pentathiophene Butyric Acid Monolayer. *Phys. Rev. B* **2013**, *87*, 205117.
(31) Elstner, M.; Porezag, D.; Jungnickel, G.; Elsner, J.; Haugk, M.; Frauenheim, T.; Suhai, S.; Seifert, G. Self-Consistent-Charge Density-Functional Tight-Binding Method for Simulations of Complex Materials Properties. *Phys. Rev. B* **1998**, *58*, 7260−7268.
(32) Niehaus, T. A.; Suhai, S.; Della Sala, F.; Lugli, P.; Elstner, M.; Seifert, G.; Frauenheim, T. Tight-Binding Approach to Time-Dependent Density-Functional Response Theory. *Phys. Rev. B* **2001**, *63*, 085108.
(33) Elstner, M. The SCC-DFTB Method and its Application to Biological Systems. *Theor. Chem. Acc.* **2006**, *116*, 316−325.
(34) Rapacioli, M.; Simon, A.; Dontot, L.; Spiegelman, F. Extensions of DFTB to Investigate Molecular Complexes and Clusters. *Phys. Status Solidi B* **2012**, *249*, 245−258.
(35) Seifert, G.; Joswig, J. Density-Functional Tight Binding—an Approximate Density-Functional Theory Method. *Wiley Interdiscip. Rev.: Comput. Mol. Sci.* **2012**, *2*, 456−465.
(36) Niehaus, T. A.; Della Sala, F. Range Separated Functionals in the Density Functional Based Tight-Binding Method: Formalism. *Phys. Status Solidi B* **2012**, *249*, 237−244.
(37) Barone, V.; Carnimeo, I.; Scalmani, G. Computational Spectroscopy of Large Systems in Solution: The DFTB/PCM and TD-DFTB/PCM Approach. *J. Chem. Theory Comput.* **2013**, *9*, 2052−2071.
(38) Gaus, M.; Goez, A.; Elstner, M. Parametrization and Benchmark of DFTB3 for Organic Molecules. *J. Chem. Theory Comput.* **2013**, *9*, 338−354.
(39) Woiczikowski, P. B.; Kubar, T.; Gutierrez, R.; Caetano, R. A.; Cuniberti, G.; Elstner, M. Combined density functional theory and Landauer approach for hole transfer in DNA along classical molecular dynamics trajectories. *J. Chem. Phys.* **2009**, *130*, 215104.
(40) Gutierrez, R.; Caetano, R. A.; Woiczikowski, B. P.; Kubar, T.; Elstner, M.; Cuniberti, G. Charge Transport through Biomolecular Wires in a Solvent: Bridging Molecular Dynamics and Model Hamiltonian Approaches. *Phys. Rev. Lett.* **2009**, *102*, 208102.
(41) Woiczikowski, P. B.; Steinbrecher, T.; Kubar, T.; Elstner, M. Nonadiabatic QM/MM Simulations of Fast Charge Transfer in Escherichia coli DNA Photolyase. *J. Phys. Chem. B* **2011**, *115*, 9846−9863.
(42) Popescu, B.; Woiczikowski, P. B.; Elstner, M.; Kleinekathofer, U. Time-Dependent View of Sequential Transport through Molecules with Rapidly Fluctuating Bridges. *Phys. Rev. Lett.* **2012**, *109*, 176802.
(43) Mitric, R.; Werner, U.; Wohlgemuth, M.; Seifert, G.; Bonacic-Koutecky, V. Nonadiabatic Dynamics within Time-Dependent Density

Functional Tight Binding Method. *J. Phys. Chem. A* **2009**, *113*, 12700−12705.
(44) Lei, Y.; Yuan, S.; Dou, Y.; Wang, Y.; Wen, Z. Detailed Dynamics of the Nonradiative Deactivation of Adenine: A Semiclassical Dynamics Study. *J. Phys. Chem. A* **2008**, *112*, 8497−8504.
(45) Zhang, W. Y.; Yuan, S. A.; Li, A. Y.; Dou, Y. S.; Zhao, J. S.; Fang, W. H. Photoinduced Thymine Dimerization Studied by Semiclassical Dynamics Simulation. *J. Phys. Chem. C* **2010**, *114*, 5594−5601.
(46) Dou, Y. S.; Yuan, S.; Zhang, W. Y.; Tang, H.; Lo, G. V. Bonded Exciplex Formation From Stacked Thymine and Adenine: Semiclassical Simulations. *Mol. Phys.* **2012**, *110*, 1517−1524.
(47) Gao, X.; Peng, Q.; Niu, Y.; Wang, D.; Shuai, Z. Theoretical Insight Into the Aggregation Induced Emission Phenomena of Diphenyldibenzofulvene: A Nonadiabatic Molecular Dynamics Study. *Phys. Chem. Chem. Phys.* **2012**, *14*, 14207−14216.
(48) Frauenheim, T.; Seifert, G.; Elstner, M.; Niehaus, T.; Kohler, C.; Amkreutz, M.; Sternberg, M.; Hajnal, Z.; Di Carlo, A.; Suhai, S. Atomistic Simulations of Complex Materials: Ground-State and Excited-State Properties. *J. Phys.: Condens. Matter* **2002**, *14*, 3015−3047.
(49) Frisch, M. J.; Trucks, G. W.; Schlegel, H. B.; Scuseria, G. E.; Robb, M. A.; Cheeseman, J. R.; Scalmani, G.; Barone, V.; Mennucci, B.; Petersson, G. A.; et al. *Gaussian 09*, revision D.01; Gaussian, Inc.: Wallingford, CT, 2009.
(50) Mei, J.; Bao, Z. Side Chain Engineering in Solution-Processable Conjugated Polymers. *Chem. Mater.* **2013**, *26*, 604−615.
(51) Lei, T.; Wang, J.; Pei, J. Roles of Flexible Chains in Organic Semiconducting Materials. *Chem. Mater.* **2013**, *26*, 594−603.
(52) Shuai, Z.; Liu, W.; Liang, W.; Shi, Q.; Chen, H. Theoretical Study of the Low-Lying Electronic Excited States for Molecular Aggregates. *Sci. China: Chem.* **2013**, *56*, 1258−1262.
(53) Shuai, Z.; Xu, W.; Peng, Q.; Geng, H. From Electronic Excited State Theory to the Property Predictions of Organic Optoelectronic Materials. *Sci. China: Chem.* **2013**, *56*, 1277−1284.
(54) Shi, Q.; Peng, Q.; Sun, S.; Shuai, Z. Vibration Correlation Function Investigation On the Phosphorescence Quantum Efficiency and Spectrum for Blue Phosphorescent Ir(III) Complex. *Acta Chim. Sin.* **2013**, *71*, 884−891.
(55) Brankin, R. W.; Gladwell, I. A Fortran 90 Version of RKSUITE: An ODE Initial Value Solver. *Annals Numer. Math.* **1994**, 363−375.
(56) Wang, L.; Beljonne, D.; Chen, L.; Shi, Q. Mixed Quantum-Classical Simulations of Charge Transport in Organic Materials: Numerical Benchmark of the Su-Schrieffer-Heeger Model. *J. Chem. Phys.* **2011**, *134*, 244116.
(57) Chandler, D. *Introduction to Modern Statistical Mechanics*; Oxford: New York, 1987; p 250.
(58) Collini, E.; Scholes, G. D. Coherent Intrachain Energy Migration in a Conjugated Polymer at Room Temperature. *Science* **2009**, *323*, 369−373.
(59) Hoofman, R.; Siebbeles, L.; de Haas, M. P.; Hummel, A.; Bloor, D. Anisotropy of the Charge-Carrier Mobility in Polydiacetylene Crystals. *J. Chem. Phys.* **1998**, *109*, 1885−1893.
(60) Hultell, M.; Stafstrom, S. Impact of Ring Torsion On the Intrachain Mobility in Conjugated Polymers. *Phys. Rev. B* **2007**, *75*, 104304.
(61) Hultell, M.; Stafstrom, S. Impact of Ring Torsion Dynamics On Intrachain Charge Transport in Conjugated Polymers. *Phys. Rev. B* **2009**, *79*, 014302.
(62) Hulea, I. N.; Fratini, S.; Xie, H.; Mulder, C. L.; Iossad, N. N.; Rastelli, G.; Ciuchi, S.; Morpurgo, A. F. Tunable Fröhlich Polarons in Organic Single-Crystal Transistors. *Nat. Mater.* **2006**, *5*, 982−986.
(63) Ortiz, R. P.; Facchetti, A.; Marks, T. J. High-k Organic, Inorganic, and Hybrid Dielectrics for Low-Voltage Organic Field-Effect Transistors. *Chem. Rev.* **2009**, *110*, 205−239.
(64) Bussac, M. N.; Kirova, N. Self-Trapping of Electrons at the Field-Effect Junction of a Molecular Crystal. *Phys. Rev. B* **2003**, *68*, 235312.
(65) Houili, H.; Picon, J. D.; Zuppiroli, L.; Bussac, M. N. Polarization Effects in the Channel of an Organic Field-Effect Transistor. *J. Appl. Phys.* **2006**, *100*, 023702.